A Benign synthesis of alane by the composition controlled mechanochemical reaction of sodium hydride and aluminum chloride

Ihor Hlova,[a] Jennifer F. Goldston,[a,c] Shalabh Gupta,[a*] Takeshi Kobayashi,[a] Marek Pruski,[a,c] Vitalij K. Pecharsky[a,b]

[a] Ames Laboratory, Iowa State University, Ames, IA 500011-3020, USA
[b] Department of Materials Science and Engineering, Iowa State University, Ames, IA 50011-2300, USA
[c] Department of Chemistry, Iowa State University, Ames, IA 500011-3111, USA

Email: shalabh@ameslab.gov

Abstract

Solid-state mechanochemical synthesis of alane (AlH_3) starting from sodium hydride (NaH) and aluminum chloride ($AlCl_3$) has been achieved at room temperature. The transformation pathway of this solid-state reaction was controlled by a step-wise addition of $AlCl_3$ to the initial reaction mixture that contained sodium hydride in excess of stoichiometric amount. As in the case of previously investigated LiH-$AlCl_3$ system, complete selectivity was achieved whereby formation of unwanted elemental aluminum was fully suppressed, and AlH_3 was obtained in quantitative yield. Reaction progress during each step was investigated by means of solid-state NMR and powder X-ray diffraction, which revealed that the overall reaction proceeds through a series of intermediate alanates that may be partially chlorinated. The NaH-$AlCl_3$ system present some subtle differences compared to LiH-$AlCl_3$ system particularly with respect to optimal concentrations needed during one of the reaction stages. Based on the results we postulate that high local concentrations of NaH may stabilize chlorine-containing derivatives and prevent decomposition into elemental aluminum with hydrogen evolution. Complete conversion with quantitative yield of alane was confirmed both by SSNMR and hydrogen desorption analysis.

Keywords: alane, ball milling, hydrogen storage, mechanochemistry, metathesis, solid-state NMR

1. Introduction

Uncertainties associated with sustainability of the current levels of production of crude oil and the ever-rising emissions of carbon dioxide are fueling a gradual transition to clean and renewable energy technologies, including electric propulsion of vehicles. As a result, many car manufacturers have committed to development of hydrogen fuel cell-powered vehicles. This stimulated intensive research on fully reversible solid-state hydrogen storage material(s) to supply the hydrogen required to power proton exchange membrane (PEM) fuel cells [1,2]. Challenging targets set forth by the U.S. DOE [3] both limit the list of materials potentially suitable for hydrogen storage applications and place in focus several candidates that may fulfill these stringent requirements and foster a smooth transition to hydrogen as a mainstream energy carrier.

According to recommendations of the Hydrogen Storage Engineering Center of Excellence, alane (AlH_3) is considered as one of the most prospective materials for hydrogen storage [4,5]. The compound is valued for its remarkable gravimetric and volumetric capacities of ~10 wt.% H and ~150 g H/l respectively, in addition to its low desorption onset temperature close to 100 °C and favorable and tunable kinetics [6]. Nonetheless, alane suffers from complete irreversibility at reasonably low hydrogen pressures, which remains an outstanding syntheses challenge [6]. While density functional based computational studies point to possible stabilization of alane clusters [7], and elucidate the favorable role of transition metal catalysts and vacancies in such processes [8], attempts to convert elemental Al to AlH_3 in high yields at easily achievable H_2 pressures have been unsuccessful. Furthermore, traditional methods for synthesis of AlH_3 not only require large volumes of environmentally hazardous organic solvents during the reaction but also relatively expensive lithium-containing reactants [9–13]. Despite being abundantly

present in the Earth's crust [14], lithium is in high demand due to the rapid growth of the rechargeable lithium battery industry. Hence, it would be beneficial to develop reactions and processes to synthesize alane using cheaper, more abundant, and noncritical resources. The most likely substitutes are the sodium-based precursors. Considering all available forms, sodium is three orders of magnitude more abundant than lithium, and is produced in large quantities through the electrolysis of molten sodium chloride that is readily available from seawater, brine, or crystalline NaCl [15].

A large body of work exists that describe the synthesis of alane from the reaction between alkali-metal hydrides or alanates with aluminum halide in ether solution [9–13]. This solution based metathesis reaction, also known as Schlesinger reaction, usually yields alane in the form of an adduct that is then further processed to obtained adduct-free alane. Successful preparation of AlH_3 *via* $NaAlH_4$-$AlCl_3$ reaction in ether-toluene mixture has been accomplished *via* the reaction [16]:

$$3NaAlH_4 + AlCl_3 \rightarrow 4AlH_3 + 3NaCl \quad (1)$$

which proved to be a lower-cost process and also much faster synthesis method in comparison to the traditional $LiAlH_4$-$AlCl_3$ route [10]. Another strategy used highly active $NaAlH_4$ together with $AlCl_3$ in a lower alkyl-dialkyl ether solution [17]. However, despite being less expensive, both these methods involve the use of large amounts of environmentally harmful organic solvents.

Processing and chemical related challenges associated with traditional methods, such as precise temperature control, handling of volatile organic liquids and significant loss of yields have prompted development of other syntheses routes that (1) may afford adduct-free alane [18–24]

and (2) utilize small amounts solvents or are entirely solvent-free [13–17]. We and others have recently demonstrated that these shortcomings can be partly circumvented by solvent-free mechanochemical syntheses of alane at room temperature using LiH or $LiAlH_4$ and $AlCl_3$ [20–24]. Here, we describe a room temperature mechanochemical process starting from a different hydrogen-containing precursor, namely NaH, which converts the 3NaH-$AlCl_3$ system into adduct-free alane.

2. Experimental

2.1. Materials and mechanochemical processing

As-received NaH (Aldrich, 95 %) and $AlCl_3$ (Aldrich, 99.99 %) were used as starting materials without further purification. Because of the high sensitivity of the precursors and products to moist air, manipulations at all stages were carried out in an Ar-filled glove box with the O_2 and H_2O levels controlled at less than 5 ppm. For a typical mechanochemical reaction, a total of 1–2 g of reaction mixture was weighed out in the desired molar ratio and transferred to a custom-built high-pressure milling container for use with a two-station planetary ball mill (Fritsch, Pulverisette 7). Twenty stainless steel balls (11.9 mm in dia., each weighing ~8 g) and the reaction mixture were placed into the container, which was then sealed under Ar atmosphere inside the glove box. The argon atmosphere was purged twice with zero grade H_2 (Linweld, 99.999%) before the container was finally pressurized to ca. 345 bar (5000 psi) H_2 pressure. High-energy milling was carried out for various time intervals at 300 rpm. To achieve effective milling and prevent excessive heating of the containers during milling, the milling direction was alternated every two minutes with an intermittent pause of one minute.

2.2. X-ray powder diffraction analysis

The progress of the reaction, as well as the yields and purity of the final products were monitored by powder X-ray diffraction (PXRD) analysis at room temperature on a PANalytical X'PERT powder diffractometer using Cu-$K_{\alpha 1}$ radiation in the 2θ range from 10° to 80° at a step size of 0.02°. To prevent oxidation from atmospheric oxygen and moisture, a polyimide (Kapton) film was used during the data acquisition, which resulted in an amorphous-like background in the PXRD patterns most notable in the 2θ range of 13–20°.

2.3. Solid-state NMR spectroscopy

Solid-state (SS)NMR experiments were performed at 9.4 T using an Agilent DD2 spectrometer, equipped with a 3.2-mm magic angle spinning (MAS) probe, tuned to 104.2, 105.8, and 400.0 MHz for ^{27}Al, ^{23}Na, and ^{1}H, respectively. To maximize quantitative accuracy, direct polarization (DP)MAS spectra were collected under 16 kHz MAS, using a single, short excitation pulse of 0.15 μs at an effective RF magnetic field strength of 150 kHz (corresponding to a flip angle of 8.1°) [25,26]. For ^{27}Al experiments, 1024 scans were collected with a relaxation delay of 3 s, whereas 512 scans and a delay of 15 s were employed in ^{23}Na experiments. In all cases, ^{1}H two-pulse phase-modulation (TPPM) decoupling [27] was applied at a frequency of 64 kHz throughout acquisition. The resulting ^{27}Al and ^{23}Na spectra were referenced to 1.0 *M* aqueous solutions of $Al(NO_3)_3$ and NaCl, respectively – both of which produce a single sharp signal at 0 ppm [28]. Finally, due to the air and/or moisture sensitivity of the materials studied, all samples were packed in MAS zirconia rotors in a glove box under argon atmosphere and sealed with gas-tight, double O-ring caps, as previously described.

2.4. Temperature Programmed Desorption

For thermal desorption measurements, as-prepared powder samples (~0.2 g) were pelletized and loaded in a custom-built autoclave within a glove box, followed by evacuation in an automatic Sievert's type volumetric gas sorption analyzer (PCTPro-2000, Setaram). Volume calibration of the free sample space was carried out with three helium absorption-desorption cycles over a period of 30–40 min during which time the temperature was maintained at 25 °C. During the desorption measurements, samples were heated at a rate of 4 °C/min up to 300 °C, followed by equilibration at that temperature until no further change in the pressure was noticeable. The composition of desorbed gases was analyzed by mass spectrometry using RGA100 residual gas analyzer coupled with the PCTPro-2000.

3. Results and Discussion

3.1. Determination of the initial reaction conditions

Earlier studies have demonstrated that mechanochemical synthesis of alane via metathesis reaction of $AlCl_3$ with Li precursors ($LiAlH_4$ or LiH) affords an easy and practical method of producing adduct-free AlH_3 in large quantities [21–24]. However, each precursor presents its own peculiarities in terms of reaction temperature, pressure or the composition of the reaction mixture. For example, the 3:1 molar mixture of $LiAlH_4$ and $AlCl_3$ could be converted in quantitative yields to AlH_3 only when the solid-state reaction was performed under gas pressure exceeding a threshold gas pressure at room temperature [21,22] or at 77 K [23,24]. Another variable is the milling energy, which unfavorably affects the time needed to complete the reaction [22]. Our systematic study of the LiH-$AlCl_3$ system has indicated that the reaction pathway is critically dependent on the composition of the reaction mixture. Briefly, when a stoichiometric 3:1 molar mixture is used to start the reaction, elemental Al

(Al_M) is formed irrespective of the applied gas pressure during ball milling. However, the reaction pathway leading to AlH_3 is favored only when the LiH concentration in the starting mixture is 9 moles or more per mole of $AlCl_3$ and the reaction is performed above a threshold pressure [21].

The complexity of these reactions and their uniqueness with respect to the precursors, suggest that the earlier results may not be fully applicable to the NaH-$AlCl_3$ system, which motivated our present investigation. As in case of the LiH-$AlCl_3$ system, initially reactions in the NaH-$AlCl_3$ system were performed for NaH:$AlCl_3$ molar ratios varying between 3:1 to 9:1 to determine the stoichiometry necessary to completely suppress the formation of Al_M. Accordingly, a 3:1 molar mixture of NaH and $AlCl_3$ was prepared and processed mechanochemically at 300 rpm under ca. 345 bar of H_2 pressure. After 60 min of milling (standard milling time used for all reactions unless stated otherwise) only Al_M and NaCl were obtained as major products (Eq. 1), which is in agreement with the similar reaction between LiH and $AlCl_3$.

$$3NaH + AlCl_3 \rightarrow Al + 3NaCl + 3/2\ H_2 \qquad (1)$$

The PXRD pattern for the corresponding reaction is shown in Fig. 1 (pattern a). As in the case of the LiH-$AlCl_3$ system, it was then reasoned that the presence of excess NaH in the starting mixture may be required to alter the reaction pathway by blocking the likely formation of unstable intermediates that immediately decompose to Al_M. Thus, varying ratios of NaH and $AlCl_3$ (4:1, 6:1 and 9:1) were examined, and it was observed that the optimum composition that prevents the formation of Al_M is close to 9:1 (Fig. 1, pattern c). All reactions with a lower NaH content than the determined optimum resulted in the formation of

Al_M and the presence of unreacted NaH, as shown in Fig. 1 (b) for the starting mixture of 6:1. Thereafter, the sample with 9:1 composition was reexamined at various stages of milling and the products obtained after 60 min of milling were subsequently used for further mechanochemical processing with additional $AlCl_3$ to yield AlH_3 and NaCl as final products.

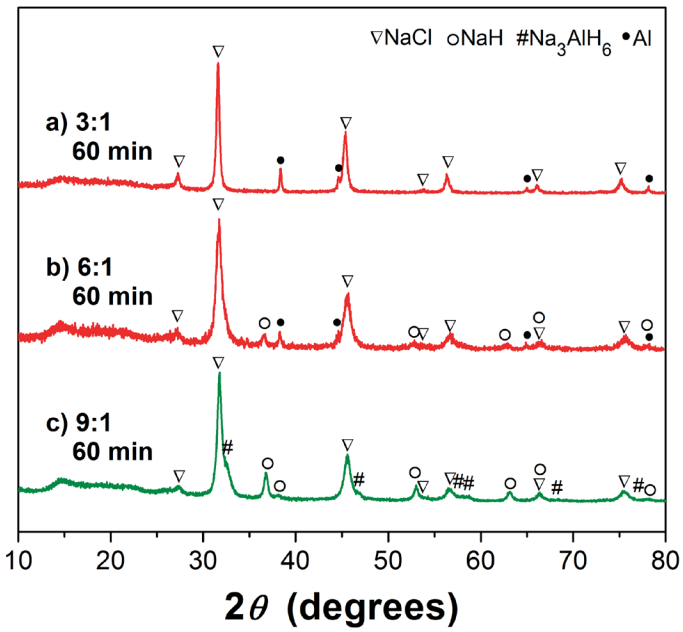

Fig. 1 Powder X-ray diffraction patterns corresponding to as-milled samples with NaH:$AlCl_3$ starting molar ratios of a) 3:1, b) 6:1 and c) 9:1 after ball milling for 60 min under 345 bar of H_2 at a milling speed of 300 rpm and ball to sample mass ratio (B/S) of ~140.

3.2. The 9:1 reaction of NaH and $AlCl_3$ (stage 1)

Once the optimal starting composition of 9NaH:1$AlCl_3$ was determined, the progress of the reaction, the formation of the intermediate compounds and the final products were analyzed by PXRD as a function of the milling time (τ_{BM}). According to the PXRD pattern shown in Fig. 2 for τ_{BM} = 4 min (pattern a), four sets of Bragg peaks are identified. Two of those sets

correspond to NaCl (with the major peaks at $2\theta \approx 32$ and 46°) [29] and orthorhombic $NaAlCl_4$ (two sets of clearly identifiable Bragg peaks are at $2\theta \approx 16$–19° and 28–32°) [30,31] as the major products. The other two sets correspond to the still unreacted NaH (with the most intense Bragg peaks at $2\theta \approx 37$ and 53°) [32] and $AlCl_3$ (the major Bragg peak is at $2\theta \approx 15°$) [33]. Upon further milling (τ_{BM} = 7 min), the peak intensities of NaH decrease and those of $AlCl_3$ disappear completely. At τ_{BM} = 10 and 15 min, the PXRD patterns clearly show the formation of $NaAlH_4$ [34] and Na_3AlH_6 [35] with a concomitant increase in NaCl and decrease in the $NaAlCl_4$ that was formed early in the reaction (Fig. 2, patterns c and d). Although the mechanism of formation of $NaAlCl_4$ is not currently understood, it is one of the most crystalline intermediates formed that could be easily observed by powder XRD. Its formation implies the concomitant presence of other ternary or quaternary intermediates, such as $AlCl_{3-x}H_x$ (x=3 or less) or Na-Al-Cl-H species (designated as phase *X* Eq. 2a):

$$NaH + AlCl_3 \rightarrow NaAlCl_4 + X \quad (2)$$

The presence of such species is difficult to confirm because of their X-ray amorphous nature, transient nature and small concentration. Identification of such species and detailed mechanistic studies require highly precise and quantitative SSNMR analysis and will be described in a separate study. Meanwhile, the presence of $NaAlH_4$ and Na_3AlH_6 after 60 minutes of milling can be explained by the following two well-known reactions [36]:

$$NaH + AlH_3 \rightarrow NaAlH_4 \quad (3a)$$

$$2NaH + NaAlH_4 \rightarrow Na_3AlH_6 \quad (3b)$$

As noted above, AlH_3 shown in the reaction (3a) most likely originate from a reaction shown in the reaction (2), which is not yet fully established because of lack of complete

characterization of the nature of products.

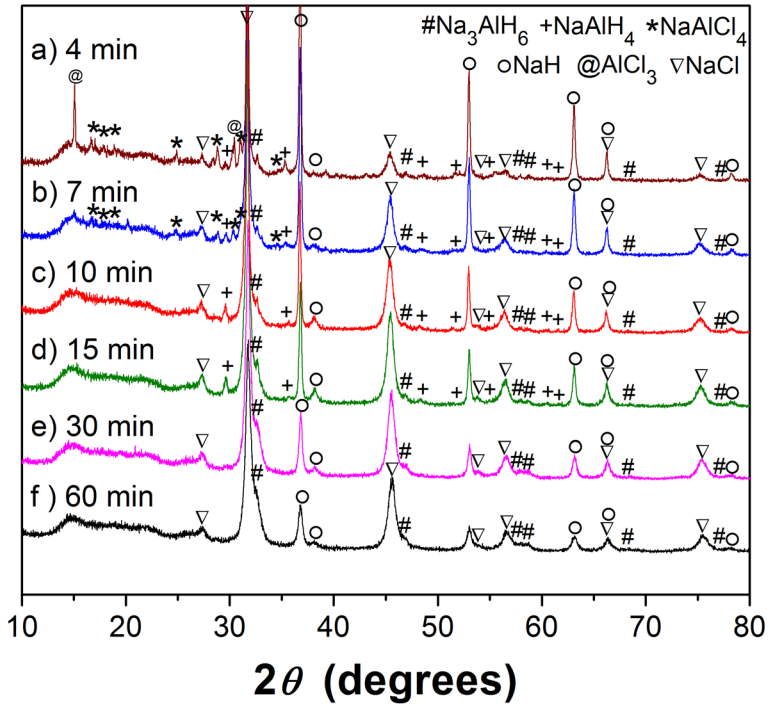

Fig. 2 Powder X-ray diffraction patterns (a-f) of samples obtained from the 9:1 mixture of NaH and $AlCl_3$ after ball-milling for the indicated time intervals under 350 bar H_2 with a milling speed of 300 rpm and a B/S of ~140. Note that this reaction corresponds to the first stage of the stepwise mechanochemical synthesis of alane, as described in the text.

After further processing (τ_{BM} = 30 and 60 min), the phases detected by PXRD are Na_3AlH_6, NaCl and unreacted NaH (Fig. 2, patterns e and f), which does not change with processing beyond 60 min indicating that the reaction has reached completion. The nearly complete consumption of $NaAlH_4$ formed early in the reaction, can likewise be understood on the basis of Eq. 3b, marking the end of stage 1.

Solid-state NMR measurements were carried out to confirm the findings from X-ray diffraction and, more importantly, to ascertain whether there were any X-ray-amorphous phase(s) are present in the sample. The ^{23}Na DPMAS spectrum of the 9:1 sample at τ_{BM} = 60 min, revealed

the presence of three different Na-containing species (Fig. 3a, stage 1). These include unreacted NaH represented by the resonance centered around 19 ppm [37], a signal originating from NaCl centered around 7 ppm, and two weak resonances at approximately 23 and –10 ppm corresponding to the two ^{23}Na sites of newly formed Na_3AlH_6 species [38]. The ^{27}Al DPMAS spectrum of the same sample (Fig. 3b, stage 1) confirms the presence of Na_3AlH_6 with an intense signal centered at –42 ppm [38]. Another hydride observed at this stage is unreacted $NaAlH_4$ (as indicated by the weak signal at ~96 ppm) [38], though this species comprises only a minor fraction of the DPMAS intensity. Thus, solid-state NMR results corroborate the PXRD analysis.

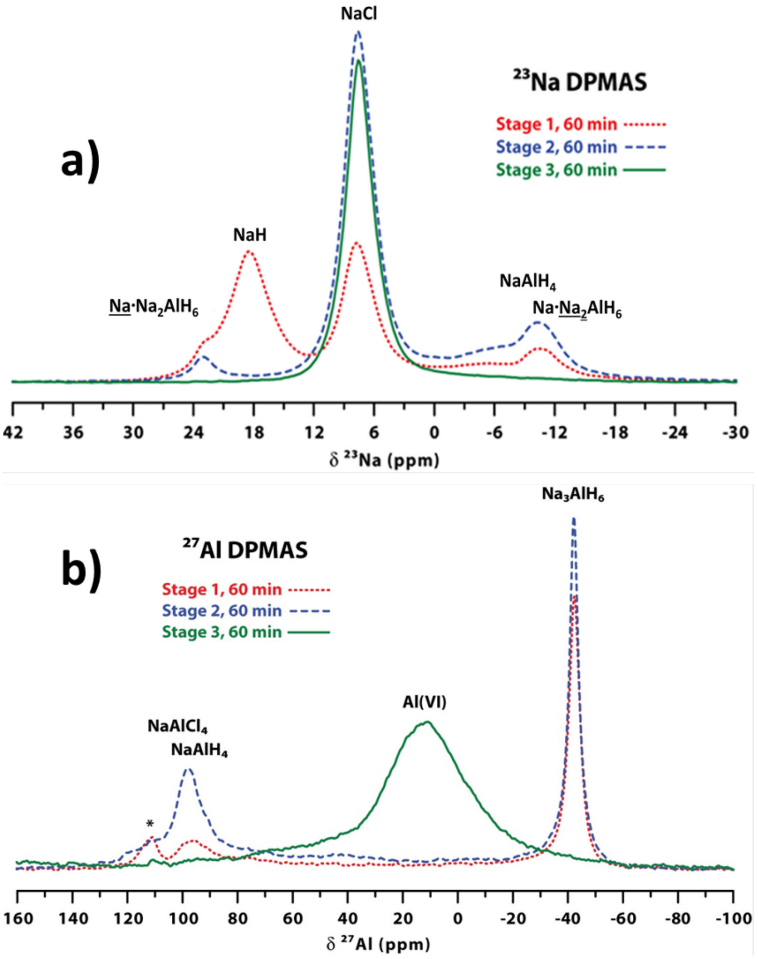

Fig. 3 ^{23}Na (a) and ^{27}Al (b) DPMAS spectra of samples obtained after each stage of processing for 60 min. Stages 1, 2 and 3 denote respectively samples with 9:1, 5:1 and 3:1 ratio of NaH:$AlCl_3$. An asterisk (*) in (b) marks a spinning sideband arising from Na_3AlH_6.

3.3. The 5:1 reaction of NaH and $AlCl_3$ (stage 2)

Further, 2 molar equivalents of $AlCl_3$ were added to the products obtained from the 9:1 reaction of NaH and $AlCl_3$ (Na_3AlH_6, NaCl and NaH at τ_{BM} = 60 min) to reach the desired NaH:$AlCl_3$ ratio of 3:1. After milling for 30 min under 345 bar of H_2, a dark grey powder was obtained, again indicating the formation of Al_M, which was also confirmed by PXRD analysis (not shown). Based on the previous experience with the LiH-$AlCl_3$ system, in a separate experiment, the amount of additional $AlCl_3$ was then reduced to 1.25 molar equivalents instead of 2 to achieve a cumulative NaH:$AlCl_3$ ratio of 4:1 rather than the target ratio of 3:1. However, contrary to the LiH-$AlCl_3$ system, this mixture still did not produce the anticipated result, and instead led to Al_M. Only when the amount of $AlCl_3$ added was reduced to 0.8 molar equivalents (resulting in an overall NaH:$AlCl_3$ ratio of 5:1), did the reaction proceed without the formation of Al_M. The progress of the 5:1 reaction was similarly monitored at same time points using PXRD, the results of which are shown in Fig. 4 and described below.

For τ_{BM} = 4 min, the PXRD data (Fig. 4, pattern a) show the Bragg peaks corresponding to the freshly formed $NaAlCl_4$ and $NaAlH_4$ and the unreacted NaH and $AlCl_3$ along with previously present NaCl and Na_3AlH_6. Upon further milling (τ_{BM} = 7–30 min), during the early period the peaks of $AlCl_3$ disappear, while peak intensities of NaH gradually decrease with concomitant increase in those corresponding to $NaAlH_4$. At a later period (τ_{BM} = 60 min), the phases detected by PXRD are $NaAlH_4$, Na_3AlH_6 and NaCl (Fig. 4, pattern f).

According to the PXRD pattern, NaH is completely consumed to produce Na_3AlH_6 according to Eq. 3b. A small portion of $NaAlH_4$ is left in the sample as the amount of NaH is now limited compared with the 9:1 reaction.

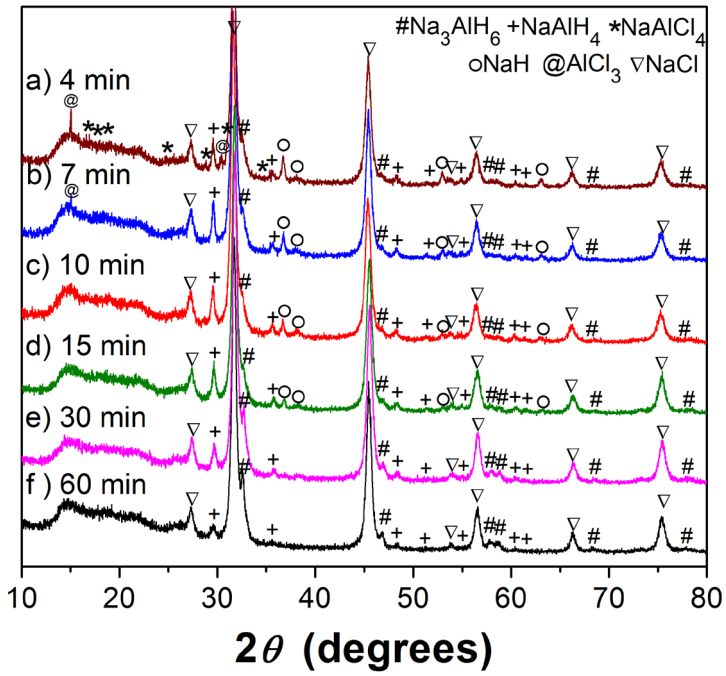

Fig. 4 Powder X-ray diffraction patterns (a-f) of samples obtained from the 5:1 mixture of NaH and $AlCl_3$ after ball-milling for the indicated time intervals under 350 bar H_2 with a milling speed of 300 rpm and a B/S of ~140. Note that this starting composition (obtained by adding 0.8 moles of $AlCl_3$ to the as-milled 9:1 products shown in Fig. 2) corresponds to the second stage of the stepwise mechanochemical synthesis of alane, as described in the text.

For the sample with τ_{BM} = 60 min, analysis of the ^{23}Na and ^{27}Al SSNMR spectra (Fig. 3, stage 2) provides consistent and comparable results to the data obtained from PXRD (Fig. 4, pattern f). In the ^{23}Na DPMAS spectrum, a strong presence of NaCl is observed at 8 ppm. The peak at ~23 ppm corresponds to one of the two ^{23}Na sites of Na_3AlH_6 species. The second site of Na_3AlH_6 at around –10 ppm, however, strongly overlaps with the signal produced by $NaAlH_4$, the presence of which is confirmed by a signal in the ^{27}Al DPMAS spectrum centered at ~96 ppm. As expected, the only other Al-containing species observed in

the ^{27}Al spectrum is Na_3AlH_6, as indicated by the intense signal at –42 ppm [38]. Thus, in the second stage, the reaction progresses through a similar set of intermediates as observed for stage 1.

3.4. The 3:1 reaction of NaH and $AlCl_3$ (stage 3)

Finally, in order to obtain alane as the end product, the remaining 1.2 molar equivalent of $AlCl_3$ was added to the mixture obtained upon completion of stage 2 of processing. Thereafter, the resulting mixture (now with what would have been a net composition of $3NaH:1AlCl_3$) was processed as in the previous two stages.

Like before, the powder XRD pattern of the products at τ_{BM} = 4 min (Fig. 5, pattern a) shows Bragg peaks corresponding to NaCl, $NaAlH_4$, and Na_3AlH_6 present from the previous stages, partially unreacted $AlCl_3$ and the newly formed $NaAlCl_4$ phase. The apparently weaker Bragg peak intensities observed for $NaAlCl_4$ in this case are because of the relatively higher concentration of NaCl now present in the sample when compared to previous stages. At τ_{BM} = 7 min (Fig. 5, pattern b), the diffraction peaks from $NaAlCl_4$ and Na_3AlH_6 vanish, whereas upon further milling (τ_{BM} = 10–30 min), the peaks corresponding to $NaAlH_4$ start to decrease as well. Finally, at τ_{BM} = 60 min, the only phase detected by PXRD is NaCl (Fig. 5, pattern f).

Although no Bragg peaks corresponding to any of the known polymorphs of alane are observed in the diffraction patterns, the absence of elemental aluminum and any starting precursors or intermediate compounds suggest that the reaction proceeded as intended, which we further corroborated by SSNMR. Indeed, the ^{23}Na DPMAS spectrum of the final product features a single peak centered at 7 ppm, representing NaCl (Fig. 3a, stage 3). A single broad

peak is also observed in the corresponding ^{27}Al DPMAS spectrum (Fig. 3b, stage 3), with the shift of ~13 ppm which is characteristic of hexa-coordinated Al. These spectra confirm that all starting precursors and intermediates have been consumed thereby unambiguously confirming the completion of the reaction. The observed ^{27}Al shift centered at ~13 ppm is broad and includes the 5.8-36.0 ppm range reported for α, β, and γ polymorphs of alane by Bowman and Hwang [39], and, within experimental error, matches the value of 14.8 ppm reported by Humphries *et al* for the α′ polymorph of alane (α′-AlH_3) [40].

The absence of Bragg peaks attributable to AlH_3 implies that it is X-ray-amorphous, or nanocrystalline in nature. It is noted that as follows from X-ray powder diffraction, the crystallinity of alane synthesized by mechanochemical metathesis at room temperature is sensitive to the milling conditions e.g. the time of milling and the process control agent(s) used during the reaction. In our previous work on $LiAlH_4$-$AlCl_3$ system [22], 3:1 molar reactions carried out at room temperature under high gas pressure yield a well-crystallized α-alane after 60 min. However, when the same reaction is carried out under ambient pressure, lower milling intensity required to avoid formation of metallic Al leads to a nearly 10-fold increase in the reaction time. The final product is identified as x-ray amorphous alane by SSNMR present in quantitative yield as determined by volumetric analysis during H_2 desorption [22]. Further, room temperature mechanochemical reactions with excess $LiAlH_4$ (e.g. 4:1–6:1 molar) produce a highly crystalline alane, which shows ^{27}Al NMR signals [41] that are in an excellent agreement with the results reported here. Finally, similar metathesis reactions, particularly with $LiAlH_4$ and $NaAlH_4$ at liquid N_2 temperature, yield alane with better crystallinity [23, 42] compared to room temperature milling under high gas pressure [22].

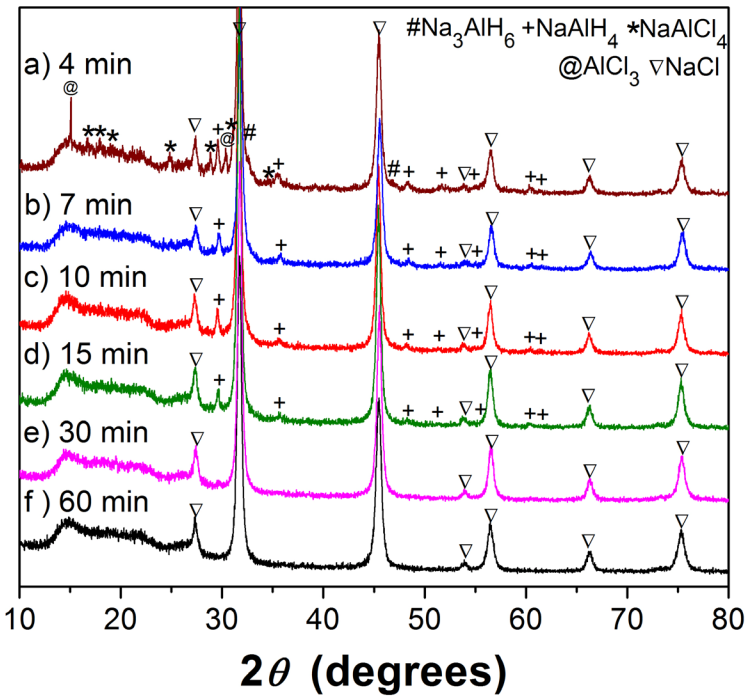

Fig. 5 Powder X-ray diffraction patterns (a-f) of samples obtained from the 3:1 mixture of NaH and $AlCl_3$ after ball-milling for the indicated time intervals under 350 bar H_2 with a milling speed of 300 rpm and a B/S of ~140. Note that this starting composition (obtained by adding 1.2 moles of $AlCl_3$ to the as-milled 5:1 products shown in Fig. 4) corresponds to the third and final stage of the stepwise mechanochemical synthesis of alane, as described in the text.

3.5. Overall reaction scheme

Based on the PXRD and SSNMR characterization, the reaction progress as studied for the indicated compositions (optimized for each step to prevent decomposition to elemental Al) may be summarized as follows:

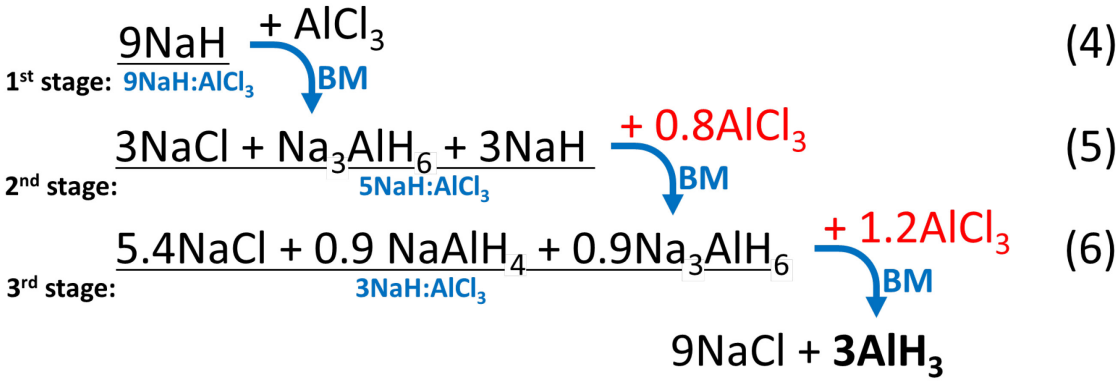

3.6. Temperature-programmed desorption (TPD) analysis

Judging only by the color of the sample, it is evident that all, or at least the majority of hydrogen is retained throughout the three stages of milling. As noted elsewhere [21,22], any loss of hydrogen during the solid-state metathesis reaction of an alkali metal hydride or alanate with aluminum halide salts results in the formation of elemental aluminum, which imparts dark gray color to the sample. In the present work, during the entire course of the reaction, the 9:1 and subsequent 5:1 and 3:1 reaction mixtures maintained a grayish white to light grey color indicating that very little, if any, elemental Al had formed. To further confirm the amount of hydrogen present in the sample after completion of each step, the volumetric desorption experiments were performed. Figure 6 (plots a, b and c) compares the decomposition profiles of the products obtained after each stage of processing at τ_{BM} = 60 min. For the 9:1 sample obtained after the first stage, a single-step desorption curve with an onset desorption temperature (T_d) of ≈ 225 °C, is in excellent agreement with the T_d reported for pristine Na_3AlH_6 [43]. The measured equilibrium hydrogen content of *ca.* 0.81 wt.% H is in nearly quantitative agreement with the ratio of the products described in Eq. 4 (3NaCl + Na_3AlH_6 + 3NaH) that altogether are expected to release 0.85 wt.% H, considering that the decomposition of NaH can only occur at temperatures exceeding 450 °C [44].

The products obtained after the second stage of processing represented by Eq. 5 (Fig. 6 plot b) have a two-step decomposition profile with T_d's close to 200 °C and 230 °C. This is also in an excellent agreement with the decomposition pathway of $NaAlH_4$ which proceeds as a two-step reaction below 400 °C [45]:

$$NaAlH_4 \rightarrow {}^{1}/_{3}Na_3AlH_6 + {}^{2}/_{3}Al + H_2 \qquad (T_d \approx 190\ °C)$$

$${}^{1}/_{3}Na_3AlH_6 \rightarrow NaH + {}^{1}/_{3}Al + {}^{1}/_{2}H_2 \qquad (T_d \approx 225\ °C)$$

$$NaH \rightarrow Na + {}^{1}/_{2}H_2 \qquad (T_d > 450\ °C)$$

The net hydrogen evolution of 1.14 wt.% hydrogen matches the expected value of 1.19 wt.% hydrogen, assuming that the reaction described by Eq. 5 proceeds to completion ($5.4NaCl + 0.9NaAlH_4 + 0.9Na_3AlH_6$). It should be noted that the first dehydrogenation step is not distinctly noticeable, mainly due to a sluggish desorption kinetics of $NaAlH_4$ [43].

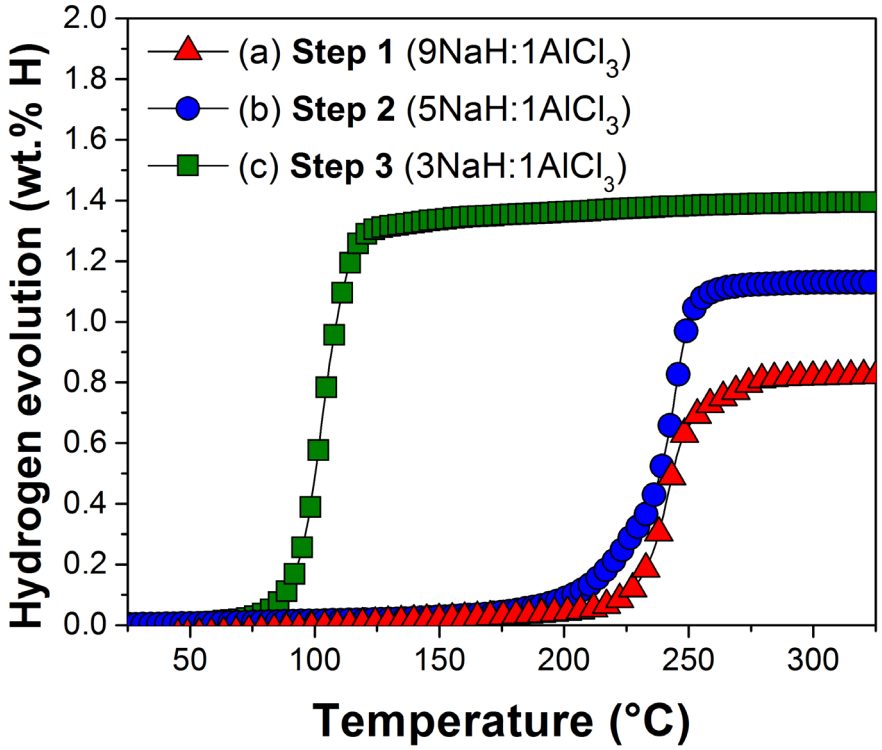

Fig. 6 Temperature-programmed desorption profiles obtained for samples of the reaction mixtures resulting from NaH:$AlCl_3$ starting ratios of (a) 9:1 (b) 5:1, and (c) 3:1 after 60 min of ball milling under 350 bar H_2 with a milling speed of 300 rpm and a B/S of ~140. Samples correspond (respectively) to the final products obtained upon completion of the first, second, and final stages of the stepwise mechanochemical synthesis of alane, as described in the text and shown in Eqs 2, 3, and 4.

Finally, curve (c) in Fig. 6 represents the decomposition profile of the products from the reaction described in Eq. 6. The one-step decomposition with a T_d of ca. 90 °C is as typically expected for AlH_3 [46], and the measured hydrogen capacity corresponding to 1.39 wt.% hydrogen is practically quantitative for the 3:1 molar mixture of NaCl and AlH_3 (1.46 wt. % H). Based on the desorption results and taking into account the observed evolution of the reaction products after the final addition of $AlCl_3$ (Figs. 3 and 5), which confirms the complete consumption of $AlCl_3$ between 4 and 7 min of the milling and eventual appearance and consumption of intermediate alanates, we confirm that hydrogen evolution occurs from alane formed mechanochemically rather than from possible thermally-induced reactions of alanates and $AlCl_3$ during heating. In all three cases, mass-spectroscopic analyses showed that H_2 constituted 99.7 % or more of the gases released, the rest being residual air.

The powder XRD analyses of desorbed samples from first and second stages of processing showed the Bragg peaks corresponding to elemental Al, NaH and NaCl (Fig. 7, patterns a and b). However, the final stage sample after desorption shows only elemental Al and NaCl (Fig. 7, pattern c), which suggests that NaH was completely consumed during the mechanochemical processing and that all of the alanates formed as intermediates during the first two stages were transformed into alane.

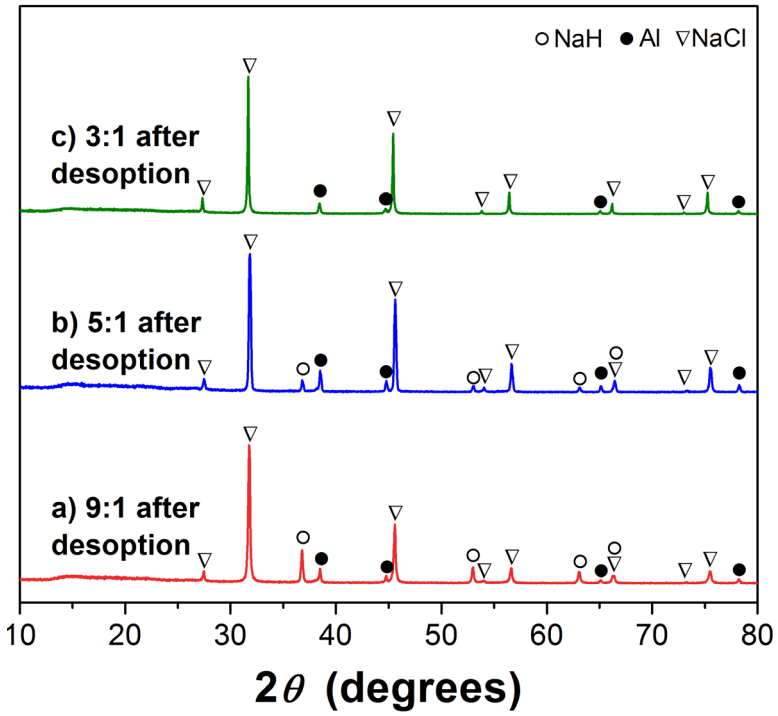

Fig. 7 Powder X-ray diffraction patterns of products obtained after complete desorption (see Fig. 6) of as-synthesized samples with (a) 9:1, (b) 5:1 and (c) 3:1 molar ratio of NaH and $AlCl_3$.

Finally, although a nearly quantitative conversion of $AlCl_3$ to alane can be achieved in a relatively simple solvent-free process, the product of the mechanochemical synthesis contains 75 mol. % (85.4 wt.%) of sodium chloride as a byproduct. Even though NaCl is benign, it must be separated from alane before the latter can be used as high-capacity source of hydrogen. While the separation of alane from NaCl is not the focus of this work, both chemical and physical separations should be possible. Apart from solvent-extraction of AlH_3, more benign physical separation techniques based on difference in densities of alane (1.49 g/cm^3) and NaCl (2.16 g/cm^3) should be possible.

3.7. Reaction mechanisms

Apparently, the presence of excess hydride source in a starting mixture can prevent decomposition to elemental Al and facilitate formation of the desired products. Similar

observations were made by Mikheeva *et al*. during their studies of the reaction between LiH and $AlCl_3$ in ethereal solution, who noticed that slow addition of $AlCl_3$ prevented decomposition of newly formed alane and improved the yield of $LiAlH_4$ [47]. Hence, similar to the previously described LiH-$AlCl_3$ system [21], the possible explanation of why the reaction between NaH and $AlCl_3$ in a 3:1 molar ratio leads to elemental Al is because of the relatively low fraction of the hydride source in the 3:1 mixture (compared to 9:1), which may not be sufficiently dispersed, leading to high local $AlCl_3$:NaH ratios. Consequently, this may cause the decomposition of unstable chlorine-containing derivatives (*e.g.* $AlCl_2H$ and $AlClH_2$ or others that are not known) into elemental aluminum with hydrogen evolution, rather than formation of intermediate alanates $NaAlH_4$ and Na_3AlH_6.

4. Conclusions

An efficient solvent-free mechanochemical method for the preparation of alane from NaH and $AlCl_3$ at room temperature has been developed. The reaction pathway could be altered by use of excess hydride source or in other word by limiting the concentration of $AlCl_3$ in the reaction mixture, thereby completely suppressing the decomposition to elemental Al and favoring the formation of the desired product AlH_3 through a series of stable alanate intermediates. Although this reaction can be carried out in organic solvents such as ether-toluene mixtures, the mechanochemical approach affords a straightforward room-temperature approach for the large-scale production of unsolvated alane. As a final note, while the concept of limiting reagent is well-known and has been widely used by chemists and biochemists to control the course of the reaction, it has not been as frequently utilized in the solid-state chemistry research. We believe this concept, as exemplified in the present work can be effectively and more generally applied to other classes of mechanochemical reactions to control pathway and alter reaction products.

5. Acknowledgements

Research supported by the Division of Materials Sciences and Engineering of Basic Energy Sciences Program of the Office of Science of the U.S. Department of Energy under Contract No. DE-AC02-07CH11358 with Iowa State University.

6. Compliance with ethical standards

Conflict of interest

The authors declare that they have no conflict of interest.

References

1. Cipriani G, Di Dio V, Genduso F, La Cascia D, Liga R, Miceli R, Galluzzo GR (2014) Perspective on hydrogen energy carrier and its automotive applications. Int J Hydrogen Energy 39(16):8482-8494.
2. McWhorter S, Read C, Ordaz G, Stetson N (2011) Materials-based hydrogen storage: attributes for near-term, early market PEM fuel cells. Curr Opin Solid State Mater Sci 15(2):29-38.
3. US Department of Energy and Office of Energy Efficiency and Renewable Energy (2015) Fuel Cell Technologies Office: Multiyear Research Development and Demonstration Plan: Planned Program Activities for 2011–2020, p 3.3-(8-3.3-15. Available at https://energy.gov/sites/prod/files/2015/05/f22/fcto_myrdd_storage.pdf
4. Brooks KP, Semelsberger TA, Simmons KL, van Hassel B (2014) Slurry-based chemical hydrogen storage systems for automotive fuel cell applications. J Power Sources 268:950-959.
5. Klebanoff L, Keller J (2012) Final report for the DOE metal hydride center of excellence. Sandia National Laboratories, Albuquerque, NM, Report No. SAND2012-0786.
6. Graetz J, Reilly JJ, Yartys VA, Maehlen JP, Bulychev BM, Antonov VE, Tarasov BP, Gabis IE (2011) Aluminum hydride as a hydrogen and energy storage material: past, present and future. J Alloys Compd 509:S517-S528.
7. Xu B, Liu J, Zhao L, Yan L (2013) Theoretical study on the structure and stability of aluminum hydride ($Al_n H_{3n}$) clusters. J. Mater. Sci. 48(6):2647–2658.
8. Wang L-L, Herwadkar A, Reich JM, Johnson DD, House SD, Pena-Martin P, Rockett AA, Robertson IM, Gupta S, Pecharsky VK (2016) Towards direct synthesis of alane: A

predicted defect-mediated pathway confirmed experimentally. Chemsuschem. 9(17):2358-2364.

9. Brower FM, Matzek NE, Reigler PF, Rinn HW, Roberts CB, Schmidt DL, Snover JA, Terada K (1976) Preparation and properties of aluminum hydride. J Am Chem Soc 98(9):2450-2453.
10. Finholt AE, Bond Jr AC, Schlesinger HI (1947) Lithium aluminum hydride, aluminum hydride and lithium gallium hydride, and some of their applications in organic and inorganic chemistry. J Am Chem Soc 69(5):1199-1203.
11. Sinke GC, Walker LC, Oetting FL, Stull DR (1967) Thermodynamic properties of aluminum hydride. J Chem Phys 47(8):2759-2761.
12. Chizinsky G, Evans GG, Gibb Jr TR, Rice Jr MJ (1955) Non-solvated aluminum hydride. J Am Chem Soc 77(11):3164-3165.
13. Matzek N, Musinski D (1974) Aluminum hydride in hexagonal or rhombohedral crystalline form. U.S. Patent No. 3,819,819.
14. Wikipedia, Abundance of elements in Earth's crust. Available at https://en.wikipedia.org/wiki/Abundance_of_elements_in_Earth's_crust
15. Klemm A, Hartmann G, Lange L (2012) Sodium and sodium alloys. Ullmann's Encyclopedia of Industrial Chemistry.
16. Kraus T, Scardera M (1974) Preparation of AlH_3 via $NaAlH_4$-AlH_3 in ether-toluene. U.S. Patent No. 3,857,930.
17. Ashby E, Taylor W, Winkler D (1974) Aluminum hydride product. U.S. Patent No. 3,829,390.

18. Bulychev BM, Verbetskii VN, Storozhenko PA (2008) “Direct” synthesis of unsolvated aluminum hydride involving Lewis and Bronsted acids. Russ J Inorg Chem 53(7):1000-1005.

19. Dinh LV, Knight DA, Paskevicius M, Buckley CE, Zidan R (2012) Novel methods for synthesizing halide-free alane without the formation of adducts. Appl Phys A 107(1):173-181.

20. Duan C, Hu L, Sun Y, Zhou H, Yu H (2015) An insight into the process and mechanism of a mechanically activated reaction for synthesizing AlH_3 nano-composites. Dalton T 44(37):16251-16255.

21. Hlova IZ, Gupta S, Goldston JF, Kobayashi T, Pruski M, Pecharsky VK (2014) Dry mechanochemical synthesis of alane from LiH and $AlCl_3$. Faraday Discuss 170:137-153.

22. Gupta S, Kobayashi T, Hlova IZ, Goldston JF, Pruski M, Pecharsky VK (2014) Solvent-free mechanochemical synthesis of alane, AlH_3: effect of pressure on the reaction pathway. Green Chem 16(9):4378-4388.

23. Brinks HW, Istad-Lem A, Hauback BC (2006) Mechanochemical Synthesis and Crystal Structure of α’-AlD_3 and α-AlD_3. J Phys Chem B 110(51):25833-25837.

24. Paskevicius M, Sheppard DA, Buckley CE (2009) Characterization of mechanochemically synthesized alane (AlH_3) nanoparticles. J Alloys Compd 487(1):370-376.

25. Wiench JW, Balema VP, Pecharsky VK, Pruski M (2004) Solid-state ^{27}Al NMR investigation of thermal decomposition of $LiAlH_4$. J Solid State Chem 177(3):648-653.

26. Freude ED, Haase J (1993) Quadrupole effects in solid-state nuclear magnetic resonance. NMR-Basic Princ Prog 29:1-90.

27. Bennett AE, Rienstra CM, Auger M, Lakshmi KV, Griffin RG (1995) Heteronuclear decoupling in rotating solids. J Chem Phys 103:6951-6958.

28. Harris RK, Becker ED, Cabral De Menezes SM, Granger P, Hoffman RE, Zilm KW (2008) Further conventions for NMR shielding and chemical shifts (IUPAC recommendations 2008). Pure Appl Chem 80:59-84.

29. The International Center for Diffraction Data (2014) PDF-00-005-0628.

30. The International Center for Diffraction Data (2014) PDF-00-023-0649.

31. Baenziger NC (1951) The crystal structure of $NaAlCl_4$. Acta Crystallogr 4(3):216-219.

32. The International Center for Diffraction Data (2014) PDF-00-054-0409.

33. The International Center for Diffraction Data (2014) PDF-00-022-0010.

34. The International Center for Diffraction Data (2014) PDF-00-022-1337.

35. The International Center for Diffraction Data (2014) PDF-00-042-0786.

36. Huot J, Boily S, Güther V, Schulz R (1999) Synthesis of Na_3AlH_6 and Na_2LiAlH_6 by mechanical alloying. J Alloys Compd 283(1-2):304-306.

37. Singh NK, Kobayashi T, Dolotko O, Wiench JW, Pruski M, Pecharsky VK (2012) Mechanochemical transformations in $NaNH_2$-MgH_2 mixtures. J Alloys Compd 513:324-327.

38. Dolotko O, Zhang H, Ugurlu O, Wiench JW, Pruski M, Chumbley LS, Pecharsky VK (2007) Mechanochemical transformations in Li(Na)AlH_4-Li(Na)NH_2 systems. Acta Mater 55(9):3121-3130.

39. Bowman RC, Hwang JC (2006) Nuclear magnetic resonance studies of hydrogen storage materials. Mater Matter 2(2): 29-31.

40. Humphries TD, Munroe KT, DeWinter TM, Jensen CM, McGrady GS (2013) NMR spectroscopic and thermodynamic studies of the etherate and the α, α′, and γ phases of AlH_3. Int J Hydrogen Energy 38(11):4577-4586.

41. Gupta S, Pecharsky VK, Kobayashi T, Pruski M, Hlova I (2015) Mechanochemical synthesis of alane PCT application WO2015123438 A1

42. Sartori S, Istad-Lem A, Brinks HW, Hauback BC (2009) Mechanochemical synthesis of alane. Int. J. Hydrogen Energy 34(15):6350-6356.

43. Beattie SD, McGrady GS (2009) Hydrogen desorption studies of $NaAlH_4$ and $LiAlH_4$ by in situ heating in an ESEM. Int J Hydrogen Energy 34(22): 9151-9156.

44. Zaluska A, Zaluski L, Ström-Olsen JO (2000) Sodium alanates for reversible hydrogen storage. J Alloys Compd 298(1):125-134.

45. Varin RA, Czujko T, Wronski ZS (2009) Nanomaterials for solid state hydrogen storage. Springer Science & Business Media.

46. Sandrock, G, Reilly J, Graetz J, Zhou WM, Johnson J, Wegrzyn J (2005) Accelerated thermal decomposition of AlH_3 for hydrogen-fueled vehicles. J Appl Phys A 80(4):687-690.

47. Mikheeva VI, Fedneva EM, Shnitkova ZL (1956) The reaction between aluminum chloride and lithium hydride in organic solvents. Zh Neorg Khim 1(11):8-19.